

Investigating the hidden-charm and hidden-bottom pentaquark resonances in scattering process.

Hongxia Huang* and Jialun Ping†

Department of Physics, Nanjing Normal University, Nanjing, Jiangsu 210097, China

In the framework of quark delocalization color screening model, both the hidden-charm and hidden-bottom pentaquark resonances are studied in the hadron-hadron scattering process. A few narrow pentaquark resonances with hidden-charm above 4.2 GeV, and some narrow pentaquark resonances with hidden-bottom above 11 GeV are found from corresponding scattering processes. Besides, the states $N\eta_c$, NJ/ψ , $N\eta_b$ and $N\Upsilon$ with $IJ^P = \frac{1}{2}\frac{1}{2}^-$, as well as NJ/ψ and $N\Upsilon$ with $IJ^P = \frac{1}{2}\frac{3}{2}^-$ are all possible to be bound by channel-coupling calculation. All these heavy pentaquarks are worth searching in the future experiments.

PACS numbers: 13.75.Cs, 12.39.Pn, 12.39.Jh

I. INTRODUCTION

In 2003, the LEPS Collaboration announced the observation of the pentaquark Θ^+ [1], which inspired a lot of theoretical work, as well as experimental work to search for pentaquarks. However, this state was not confirmed by the subsequent more advanced experiments. Nevertheless, the LEPS Collaboration still insists on the existence of pentaquark Θ^+ [2], and the relevant experiment is also in progress [3]. Moreover, there were also some theoretical studies on the existence of the hidden-charm pentaquarks [4–12]. In the year of 2015, the claim of two hidden-charm pentaquark states $P_c(4380)$ and $P_c(4450)$ by the LHCb Collaboration [13] attracted people's interesting in the pentaquarks again and triggered more and more theoretical work on these two states. Until now, theoretical interpretations of $P_c(4380)$ and $P_c(4450)$ include the baryon-meson molecules [14–23], the diquark-triquark pentaquarks [24, 25], the diquark-diquark-antiquark pentaquarks [26–29], the genuine multiquark states [30], the topological soliton [31], and the kinematical threshold effects in the triangle singularity mechanism [32–34], etc. The more comprehensive discussions on the current experimental progresses and various theoretical interpretations of these candidates can be found in Ref. [35].

To provide the necessary information for experiments to search for multiquark states, mass spectrum calculation alone is not enough. The calculation of hadron-hadron scattering, the main production process of multiquark states, is indispensable. The scattering phase shifts will show a resonance behavior in the resonance energy region. In many theoretical work mentioned above, they investigated $P_c(4380)$ and $P_c(4450)$ as bound states. In fact, these states will decay through the related open channels. As we mentioned in our previous work [18], in the bound-state calculation $P_c(4380)$ can be explained

as the molecular pentaquark Σ_c^*D with the quantum number $J^P = \frac{3}{2}^-$, but it can decay to the open channels NJ/ψ and $\Lambda_c D^*$. Therefore, we should study the NJ/ψ and $\Lambda_c D^*$ scattering process to check whether the $P_c(4380)$ is a resonance state or not. Similar work has been done in the dibaryon system, in which we obtained the d^* resonance during the NN scattering process, and found that the energy and decay width of the partial wave of NN were consistent with the experiment data [36]. Extending to the pentaquark system, we investigated the $N\phi$ state in the different scattering channels: $N\eta'$, ΛK , and ΣK [37]. Both the resonance mass and decay width were obtained, which provided the necessary information for experimental searching at Jefferson Lab. Therefore, it is interesting to extend such study to the molecular pentaquarks with heavy quarks.

Generally, hadron structure and hadron interactions belong to the low energy physics of quantum chromodynamics (QCD), which are much harder to calculate directly from QCD because of the non-perturbative nature of QCD. One has to rely on effective theories and/or QCD-inspired models to get some insight into the phenomena of the hadronic world. The constituent quark model is one of them, which approximately transforms the complicated interactions between current quarks into dynamic properties of quasiparticles (constituent quark) and considers the residual interactions between quasiparticles. There are various kinds of constituent quark models, such as one-boson-exchange model, chiral quark model, quark delocalization color screening model (QDCSM), and so on. These models have been successful in describing hadron spectrum, the baryon-baryon interactions and the bound state of two baryons, the deuteron. Among these phenomenological models, QDCSM, which was developed in the 1990s with the aim of explaining the similarities between nuclear (hadronic clusters of quarks) and molecular forces [38], was extensively used and studied in our group. In this model, quarks confined in one cluster are allowed to delocalize to a nearby cluster and the confinement interaction between quarks in different clusters is modified to include a color screening factor. The latter is a model description of the hidden color

*Electronic address: hxhuang@njnu.edu.cn

†Electronic address: jlping@njnu.edu.cn

channel coupling effect [39]. The delocalization parameter is determined by the dynamics of the interacting multi-quark system, thus allows the system to choose the most favorable configuration through its own dynamics in a larger Hilbert space. Recently, this model has been used to study the hidden-charm pentaquarks [18]. We found that the interaction between Σ_c (or Σ_c^*) and D (or D^*) was strong enough to form some bound states, and $P_c(4380)$ can be interpreted as the molecular state Σ_c^*D with quantum numbers $IJ^P = \frac{1}{2}\frac{3}{2}^-$. In this work, we continue to study the hidden-charm resonance states in the related hadron-hadron scattering process. Besides, we also extend the study to the hidden bottom sector to search for the some hidden-bottom pentaquark resonances.

In the next section, the framework of the QDCSM and the calculation method are briefly introduced. Section III devotes to the numerical results and discussions. The summary is shown in the last section.

II. QUARK MODEL AND THE CALCULATION METHOD

Since our previous work of the bound-state calculation of the hidden-charm molecular pentaquark [18] was

carried through our quark delocalization color screening model (QDCSM), we use the same model and parameters to study the pentaquark resonances here. Besides, to calculate the baryon-meson scattering phase shifts and to observe the resonance states, the well developed resonating group method (RGM) [40] is used.

A. Quark delocalization color screening model

The detail of QDCSM used in the present work can be found in the references [38, 39, 41]. Here, we just present the salient features of the model. The model Hamiltonian is:

$$\begin{aligned}
 H &= \sum_{i=1}^5 \left(m_i + \frac{p_i^2}{2m_i} \right) - T_c + \sum_{i<j} [V^G(r_{ij}) + V^\chi(r_{ij}) + V^C(r_{ij})], \\
 V^G(r_{ij}) &= \frac{1}{4} \alpha_s \lambda_i \cdot \lambda_j \left[\frac{1}{r_{ij}} - \frac{\pi}{2} \left(\frac{1}{m_i^2} + \frac{1}{m_j^2} + \frac{4\sigma_i \cdot \sigma_j}{3m_i m_j} \right) \delta(r_{ij}) - \frac{3}{4m_i m_j r_{ij}^3} S_{ij} \right], \\
 V^\chi(r_{ij}) &= \frac{1}{3} \alpha_{ch} \frac{\Lambda^2}{\Lambda^2 - m_\chi^2} m_\chi \left\{ \left[Y(m_\chi r_{ij}) - \frac{\Lambda^3}{m_\chi^3} Y(\Lambda r_{ij}) \right] \sigma_i \cdot \sigma_j \right. \\
 &\quad \left. + \left[H(m_\chi r_{ij}) - \frac{\Lambda^3}{m_\chi^3} H(\Lambda r_{ij}) \right] S_{ij} \right\} \mathbf{F}_i \cdot \mathbf{F}_j, \quad \chi = \pi, K, \eta \\
 V^C(r_{ij}) &= -a_c \lambda_i \cdot \lambda_j [f(r_{ij}) + V_0], \\
 f(r_{ij}) &= \begin{cases} r_{ij}^2 & \text{if } i, j \text{ occur in the same baryon orbit} \\ \frac{1 - e^{-\mu_{ij} r_{ij}^2}}{\mu_{ij}} & \text{if } i, j \text{ occur in different baryon orbits} \end{cases} \\
 S_{ij} &= \frac{(\sigma_i \cdot \mathbf{r}_{ij})(\sigma_j \cdot \mathbf{r}_{ij})}{r_{ij}^2} - \frac{1}{3} \sigma_i \cdot \sigma_j.
 \end{aligned} \tag{1}$$

Where S_{ij} is quark tensor operator; $Y(x)$ and $H(x)$ are standard Yukawa functions [42]; T_c is the kinetic energy of the center of mass; α_{ch} is the chiral coupling constant; determined as usual from the π -nucleon coupling constant; α_s is the quark-gluon coupling constant. In order to cover the wide energy range from light to heavy quarks one introduces an effective scale-dependent quark-gluon

coupling $\alpha_s(\mu)$ [43]:

$$\alpha_s(\mu) = \frac{\alpha_0}{\ln\left(\frac{\mu^2 + u_0^2}{\Lambda_0^2}\right)}. \tag{2}$$

Where μ is the reduced mass of the interacting quarks pair. All other symbols have their usual meanings, and all parameters are taken from our previous work [18].

Besides, the quark delocalization in QDCSM is realized by specifying the single particle orbital wave function of QDCSM as a linear combination of left and right Gaussians, the single particle orbital wave functions used in the ordinary quark cluster model. One can refer to the Ref. [18] to see the orbital wave functions.

B. The calculation method

Here, we calculate the baryon-meson scattering phase shifts and investigate the resonance states by using the resonating group method (RGM) [40], a well established method for studying a bound-state problem or a scattering one. The wave function of the baryon-meson system is of the form

$$\Psi = \mathcal{A} \left[\hat{\phi}_A(\boldsymbol{\xi}_1, \boldsymbol{\xi}_2) \hat{\phi}_B(\boldsymbol{\xi}_3) \chi_L(\mathbf{R}_{AB}) \right]. \quad (3)$$

where $\boldsymbol{\xi}_1$ and $\boldsymbol{\xi}_2$ are the internal coordinates for the baryon cluster A, and $\boldsymbol{\xi}_3$ is the internal coordinate for the meson cluster B. $\mathbf{R}_{AB} = \mathbf{R}_A - \mathbf{R}_B$ is the relative coordinate between the two clusters. The $\hat{\phi}_A$ and $\hat{\phi}_B$ are the internal cluster wave functions of the baryon A (anti-symmetrized) and meson B, and $\chi_L(\mathbf{R}_{AB})$ is the relative motion wave function between two clusters. The symbol \mathcal{A} is the anti-symmetrization operator defined as

$$\mathcal{A} = 1 - P_{14} - P_{24} - P_{34}, \quad (4)$$

where 1, 2, and 3 stand for the quarks in the baryon cluster and 4 stands for the quark in the meson cluster. For a bound-state problem, $\chi_L(\mathbf{R}_{AB})$ is expanded by gaussian bases

$$\begin{aligned} \chi_L(\mathbf{R}_{AB}) &= \frac{1}{\sqrt{4\pi}} \left(\frac{6}{5\pi b^2} \right)^{3/4} \sum_{i=1}^n C_i \\ &\times \int \exp \left[-\frac{3}{5b^2} (\mathbf{R}_{AB} - \mathbf{S}_i)^2 \right] Y_{LM}(\hat{\mathbf{S}}_i) d\hat{\mathbf{S}}_i \\ &= \sum_{i=1}^n C_i \frac{u_L(R_{AB}, S_i)}{R_{AB}} Y_{LM}(\hat{\mathbf{R}}_{AB}). \end{aligned} \quad (5)$$

with

$$\begin{aligned} u_L(R_{AB}, S_i) &= \sqrt{4\pi} \left(\frac{6}{5\pi b^2} \right)^{3/4} R_{AB} \\ &\times \exp \left[-\frac{3}{5b^2} (R_{AB}^2 - S_i^2) \right] i^L j_L(-i \frac{6}{5b^2} R_{AB} S_i). \end{aligned} \quad (6)$$

where \mathbf{S}_i is called the generating coordinate, C_i is expansion coefficients, n is the number of the gaussian bases, which is determined by the stability of the results, and j_L is the L -th spherical Bessel function.

For a scattering problem, the relative wave function is expanded as

$$\chi_L(\mathbf{R}_{AB}) = \sum_{i=1}^n C_i \frac{\tilde{u}_L(R_{AB}, S_i)}{R_{AB}} Y_{LM}(\hat{\mathbf{R}}_{AB}). \quad (7)$$

with

$$\begin{aligned} \tilde{u}_L(R_{AB}, S_i) &= \\ &\begin{cases} \alpha_i u_L(R_{AB}, S_i), & R_{AB} \leq R_C \\ [h_L^-(k_{AB}, R_{AB}) - s_i h_L^+(k_{AB}, R_{AB})] R_{AB}, & R_{AB}, R_{AB} \geq R_C \end{cases} \end{aligned} \quad (8)$$

where h_L^\pm is the L -th spherical Hankel functions, k_{AB} is the momentum of relative motion with $k_{AB} = \sqrt{2\mu_{AB} E_{cm}}$, μ_{AB} is the reduced mass of two hadrons (A and B) of the open channel; E_{cm} is the incident energy, and R_C is a cutoff radius beyond which all the strong interaction can be disregarded. Besides, α_i and s_i are complex parameters which are determined by the smoothness condition at $R_{AB} = R_C$ and C_i satisfy $\sum_{i=1}^n C_i = 1$. After performing variational procedure, a L -th partial-wave equation for the scattering problem can be deduced as

$$\sum_{j=1}^n \mathcal{L}_{ij}^L C_j = \mathcal{M}_i^L \quad (i = 0, 1, \dots, n-1), \quad (9)$$

with

$$\mathcal{L}_{ij}^L = \mathcal{K}_{ij}^L - \mathcal{K}_{i0}^L - \mathcal{K}_{0j}^L + \mathcal{K}_{00}^L, \quad (10)$$

$$\mathcal{M}_i^L = \mathcal{K}_{00}^L - \mathcal{K}_{i0}^L, \quad (11)$$

and

$$\begin{aligned} \mathcal{K}_{ij}^L &= \left\langle \hat{\phi}_A(\boldsymbol{\xi}'_1, \boldsymbol{\xi}'_2) \hat{\phi}_B(\boldsymbol{\xi}'_3) \frac{\tilde{u}_L(R'_{AB}, S_i)}{R'_{AB}} Y_{LM}(\hat{\mathbf{R}}'_{AB}) \right. \\ &\quad \left. |H - E| \right. \\ &\quad \left. \mathcal{A} \left[\hat{\phi}_A(\boldsymbol{\xi}_1, \boldsymbol{\xi}_2) \hat{\phi}_B(\boldsymbol{\xi}_3) \frac{\tilde{u}_L(R_{AB}, S_j)}{R_{AB}} Y_{LM}(\hat{\mathbf{R}}_{AB}) \right] \right\rangle. \end{aligned} \quad (12)$$

By solving Eq.(9), we can obtain the expansion coefficients C_i . Then the S matrix element S_L and the phase shifts δ_L are given by

$$S_L \equiv e^{2i\delta_L} = \sum_{i=1}^n C_i s_i, \quad (13)$$

III. THE RESULTS AND DISCUSSIONS

From our previous bound-state calculation [18], for the $IJ^P = \frac{1}{2} \frac{1}{2}^-$ system, the single channel $\Sigma_c D$, $\Sigma_c D^*$ and $\Sigma_c^* D^*$ was bound; while the other four channels $N\eta_c$, NJ/ψ , $\Lambda_c D$ and $\Lambda_c D^*$ were unbound and scattering channels. For the $IJ^P = \frac{1}{2} \frac{3}{2}^-$ system, the case is similar. There are two scattering channels (NJ/ψ and $\Lambda_c D^*$) and three bound-state channels ($\Sigma_c D^*$, $\Sigma_c^* D$ and $\Sigma_c^* D^*$). These bound states may appear as resonance states in the corresponding scattering channels and acquire finite widths. We should mention that all states we study here

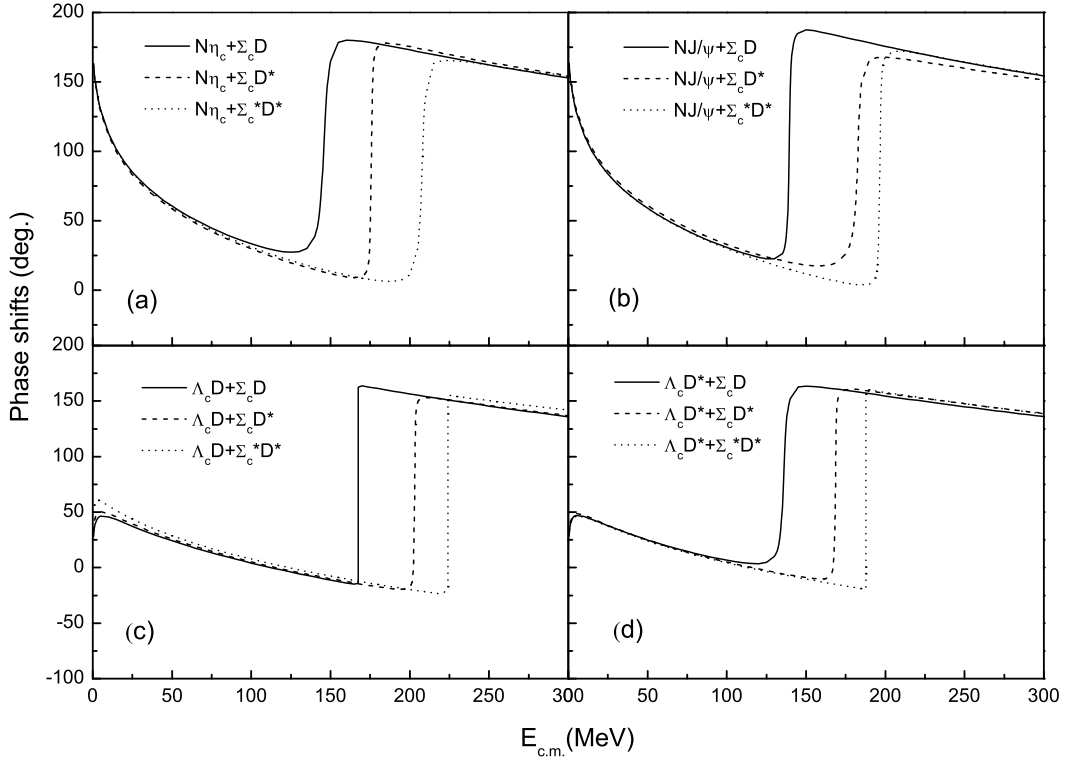


FIG. 1: The $N\eta_c$, NJ/ψ , $\Lambda_c D$ and $\Lambda_c D^*$ S -wave phase shifts with two-channel coupling for the $IJ^P = \frac{1}{2}\frac{1}{2}^-$ system.

TABLE I: The mass and decay width (in MeV) of the $IJ^P = \frac{1}{2}\frac{1}{2}^-$ resonance states in the $N\eta_c$, NJ/ψ , $\Lambda_c D$ and $\Lambda_c D^*$ S -wave scattering process.

	two-channel coupling						four-channel coupling					
	$\Sigma_c D$		$\Sigma_c D^*$		$\Sigma_c^* D^*$		$\Sigma_c D$		$\Sigma_c D^*$		$\Sigma_c^* D^*$	
	M	Γ	M	Γ	M	Γ	M	Γ	M	Γ	M	Γ
$N\eta_c$	4309.8	6.0	4451.7	1.1	4523.1	3.5	4311.3	4.5	4448.8	1.0	4525.8	4.0
NJ/ψ	4305.9	2.0	4461.6	4.0	4514.7	1.2	4307.9	1.2	4459.7	3.9	nr	–
$\Lambda_c D$	4308.4	0.003	4452.6	1.0	4512.6	0.004	4306.7	0.02	4461.6	1.0	nr	–
$\Lambda_c D^*$	4311.6	3.5	4452.5	1.0	4510.8	0.005	4307.7	1.4	4449.0	0.3	nr	–

are in S -wave because we found that there was no bound state with higher partial waves in our calculations. The S -wave bound states decay to D -wave open channels through tensor interaction are neglected here due to the small decay widths. So the total decay width of the states given below is the lower limits, also due to only the hidden-charm channels are considered in this work. Besides, we do two kinds of channel-coupling in this work. The first one is the two-channel coupling with a single bound state and a related open channel; another one is the four-channel coupling with three bound states and a corresponding open channel. The general features of the calculated results are as follows.

For the $IJ^P = \frac{1}{2}\frac{1}{2}^-$ system, we do the two-channel coupling calculation firstly. The phase shifts of all scattering channels are shown in Fig. 1. The phase shifts of

the $N\eta_c$ channel (see Fig. 1(a)) clearly show three resonance states, which means that every bound state $\Sigma_c D$, $\Sigma_c D^*$ and $\Sigma_c^* D^*$ appear as resonance state by coupling to the scattering channel $N\eta_c$. Other scattering channels NJ/ψ , $\Lambda_c D$ and $\Lambda_c D^*$ (see Fig. 1 (b), (c) and (d)) show similar results as that of $N\eta_c$. From the shape of the resonance, the resonance mass and decay width of every resonance state can be obtained, which are listed in Table I. Comparing with the result of our previous bound-state calculation [18], the mass shift of every resonance state is not very large, which indicates that the scattering channel and the bound-state channel coupling effect is not very strong although it is through the central force. The reasons is that the mass difference between the scattering channel and the bound-state channel is large, which is about 100 ~ 400 MeV.

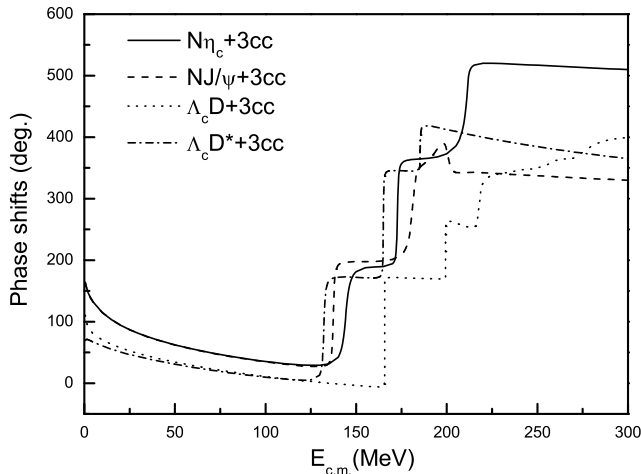


FIG. 2: The $N\eta_c$, NJ/ψ , $\Lambda_c D$ and $\Lambda_c D^*$ S -wave phase shifts with four-channel coupling for the $IJ^P = \frac{1}{2}\frac{1}{2}^-$ system.

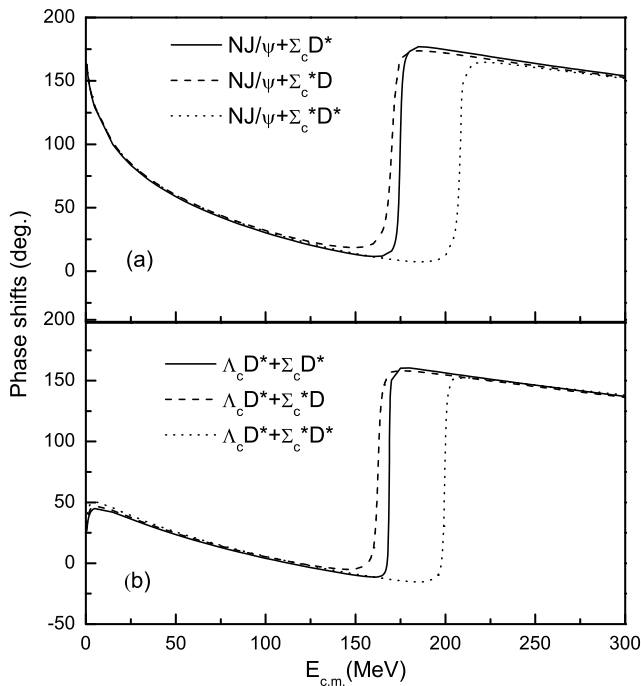


FIG. 3: The NJ/ψ and $\Lambda_c D^*$ S -wave phase shifts with two-channel coupling for the $IJ^P = \frac{1}{2}\frac{3}{2}^-$ system.

To investigate the effect of channel-coupling of the bound states, we also do the four-channel coupling calculation. The phase shifts of all scattering channels of the $IJ^P = \frac{1}{2}\frac{1}{2}^-$ system are shown in Fig. 2, which shows a multi-resonance behavior. There are three resonance states in the $N\eta_c$ scattering phase shifts, corresponding to $\Sigma_c D$, $\Sigma_c D^*$ and $\Sigma_c^* D^*$ states; while in other scattering channels, there are only two resonance states, which are $\Sigma_c D$ and $\Sigma_c D^*$. There is only a wavy motion around the threshold of the third state, $\Sigma_c^* D^*$. The reason is that the channel coupling pushes the higher state above the threshold. The resonance mass and decay width of

TABLE II: The mass and decay width (in MeV) of the $IJ^P = \frac{1}{2}\frac{3}{2}^-$ resonance states in the NJ/ψ and $\Lambda_c D^*$ S -wave scattering process.

	two-channel coupling					
	$\Sigma_c D^*$		$\Sigma_c^* D$		$\Sigma_c^* D^*$	
	M	Γ	M	Γ	M	Γ
NJ/ψ	4453.8	1.7	4379.7	4.5	4526.4	2.5
$\Lambda_c D^*$	4452.7	0.8	4377.6	3.2	4522.7	1.8
	four-channel coupling					
	$\Sigma_c D^*$		$\Sigma_c^* D$		$\Sigma_c^* D^*$	
	M	Γ	M	Γ	M	Γ
NJ/ψ	4454.0	1.5	4376.4	1.5	nr	–
$\Lambda_c D^*$	4452.0	0.3	4374.4	0.9	4523.0	1.0

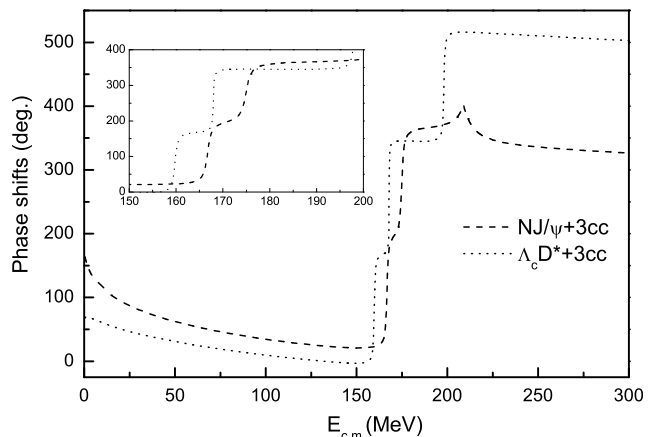


FIG. 4: The NJ/ψ and $\Lambda_c D^*$ S -wave phase shifts with four-channel coupling for the $IJ^P = \frac{1}{2}\frac{3}{2}^-$ system.

resonance states by four-channel coupling are also listed in Table I. Both $\Sigma_c D$ and $\Sigma_c D^*$ with $IJ^P = \frac{1}{2}\frac{1}{2}^-$ are resonance states in related scattering channels. The resonance mass range of $\Sigma_c D$ state is 4306.7 ~ 4311.3 MeV and the decay width is about 7.1 MeV, and $\Sigma_c D^*$ has the mass range of 4448.8 ~ 4461.6 MeV and the decay width of 6.2 MeV. $\Sigma_c^* D^*$ appears as a resonance state only in the $N\eta_c$ channel, with mass of 4525.8 MeV and decay width of 4.0 MeV. These results are qualitatively similar to the conclusion of Ref. [4], in which they predicted two new N^* states (the $\Sigma_c D$ molecular state $N^*(4265)$ and the $\Sigma_c D^*$ molecular state $N^*(4415)$) in the coupled-channel unitary approach.

Particularly, in Figs. 1 and 2, the low-energy scattering phase shifts of both $N\eta_c$ and NJ/ψ channels go to 180° at $E_{c.m.} \sim 0$ and rapidly decreases as $E_{c.m.}$ increases, which implies that both $N\eta_c$ and NJ/ψ state are bound states with the help of channel-coupling. Meanwhile, the slope of the low-energy phase shifts (near $E_{c.m.} \sim 0$) of both $\Lambda_c D$ and $\Lambda_c D^*$ is opposite to that of $N\eta_c$ and NJ/ψ channels, which means that neither $\Lambda_c D$ nor $\Lambda_c D^*$ state is bound state even with channel coupling. All these re-

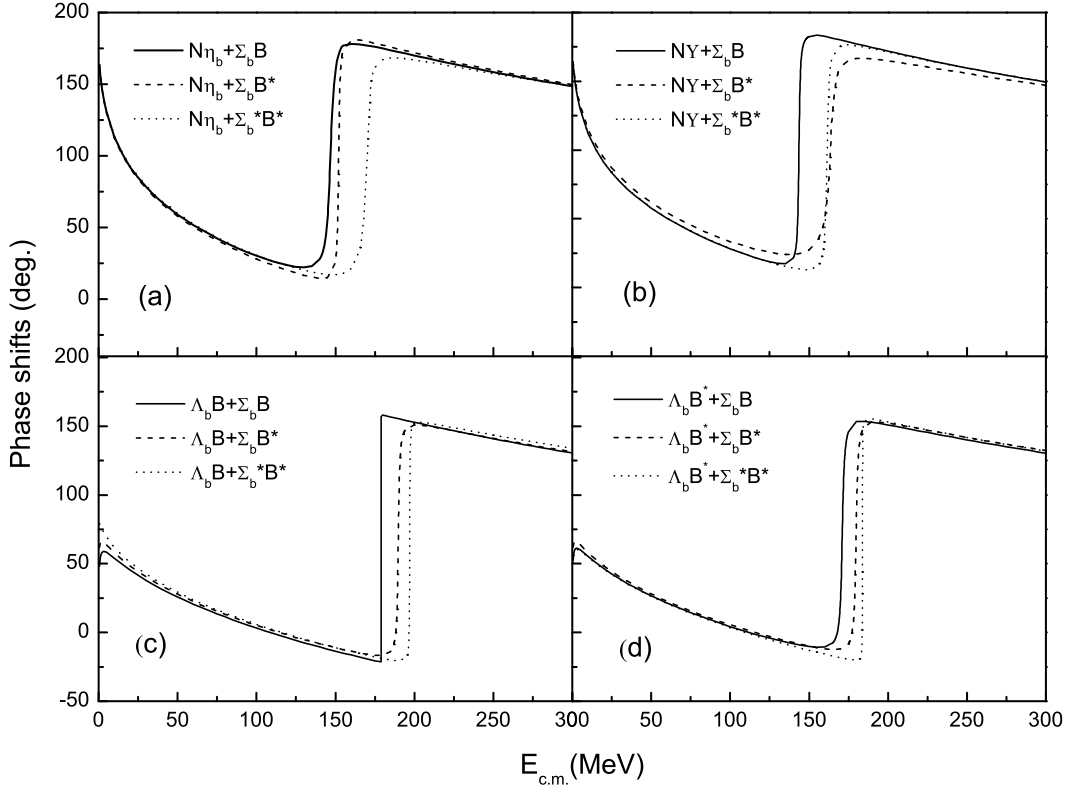


FIG. 5: The $N\eta_b$, $N\Upsilon$, $\Lambda_b B$ and $\Lambda_b B^*$ S -wave phase shifts with two-channel coupling for the $IJ^P = \frac{1}{2}\frac{1}{2}^-$ system.

TABLE III: The mass and decay width (in MeV) of the $IJ^P = \frac{1}{2}\frac{1}{2}^-$ resonance states in the $N\eta_b$, $N\Upsilon$, $\Lambda_b B$ and $\Lambda_b B^*$ S -wave scattering process.

	two-channel coupling						four-channel coupling					
	$\Sigma_b B$		$\Sigma_b B^*$		$\Sigma_b^* B^*$		$\Sigma_b B$		$\Sigma_b B^*$		$\Sigma_b^* B^*$	
	M	Γ	M	Γ	M	Γ	M	Γ	M	Γ	M	Γ
$N\eta_b$	11083.3	4.0	11123.9	1.4	11154.5	4.7	11079.8	1.2	11120.6	0.4	11156.9	2.0
$N\Upsilon$	11080.4	1.4	11135.4	6.6	11146.2	2.0	11077.5	0.1	11125.8	0.8	11153.5	3.0
$\Lambda_b B$	11079.0	0.0003	11125.4	2.0	11145.1	0.49	11077.2	0.001	11122.0	0.6	11141.8	0.1
$\Lambda_b B^*$	11082.25	2.6	11126.2	2.3	11142.7	0.22	11078.3	0.3	11123.0	1.2	11141.5	0.4

sults are consistent with our bound-state calculation [18].

For $IJ^P = \frac{1}{2}\frac{3}{2}^-$ system, the same calculation has been done and similar results are obtained. In the two-channel coupling calculation, three bound states $\Sigma_c D^*$, $\Sigma_c^* D$ and $\Sigma_c^* D^*$ all appear as resonance states in the scattering phase shifts NJ/ψ and $\Lambda_c D^*$, which are shown in Fig. 3. In the four-channel coupling calculation, the multi-resonance behavior appears again, as shown in Fig. 4. Three resonance states appear in the $\Lambda_c D^*$ scattering phase shifts, corresponding to $\Sigma_c D^*$, $\Sigma_c^* D$ and $\Sigma_c^* D^*$ states; while in NJ/ψ scattering channels, there are only two resonance states $\Sigma_c D^*$ and $\Sigma_c^* D$. The cusp in the dashed line of Fig. 4 is a remnant of the $\Sigma_c^* D^*$. The resonance mass and decay width of resonance states by two kinds of channel coupling are listed in Table II. The $\Sigma_c D^*$

is shown as a resonance state in both NJ/ψ and $\Lambda_c D^*$ scattering process with mass range of 4452.0 ~ 4454.0 MeV and decay width of 1.8 MeV; the $\Sigma_c^* D$ is also a resonance state in both NJ/ψ and $\Lambda_c D^*$ scattering channels with mass range of 4374.4 ~ 4376.4 MeV and decay width of 2.4 MeV; while $\Sigma_c^* D^*$ appears as a resonance state only in the $\Lambda_c D^*$ channel, with mass of 4523.0 MeV and decay width of 1.0 MeV. It is obvious that the mass of this resonance state $\Sigma_c^* D$ is consistent with the $P_c(4380)$, but the decay width is much smaller than the experimental data, which is about 200 MeV. As mentioned above, only the hidden-charm channels are considered in this work, so the total decay width of this state is the lower limits here. More decay channels should be considered in future work.

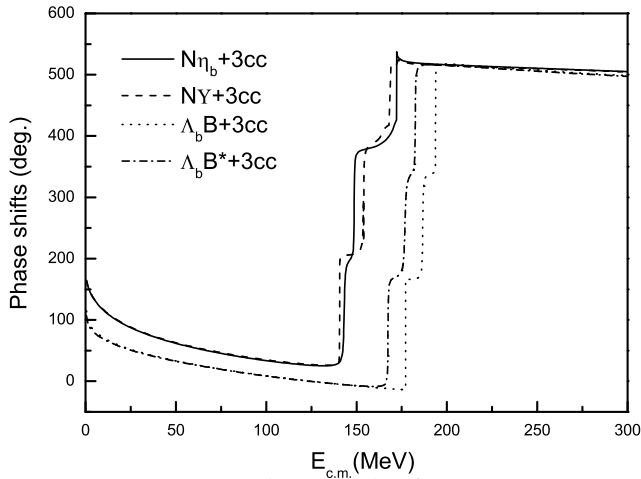


FIG. 6: The $N\eta_b$, $N\Upsilon$, $\Lambda_b B$ and $\Lambda_b B^*$ S -wave phase shifts with four-channel coupling for the $IJ^P = \frac{1}{2}\frac{1}{2}^-$ system.

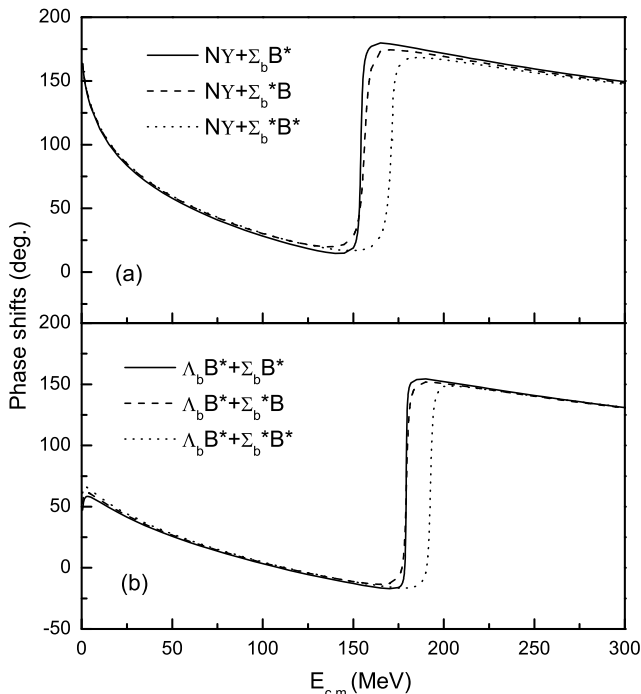


FIG. 7: The $N\Upsilon$ and $\Lambda_b B^*$ S -wave phase shifts with two-channel coupling for the $IJ^P = \frac{1}{2}\frac{3}{2}^-$ system.

Moreover, the behaviour of the low-energy phase shifts of NJ/ψ channel in both Figs. 3 and 4 is similar to that in Figs. 1 and 2. This indicates that the NJ/ψ with $IJ^P = \frac{1}{2}\frac{3}{2}^-$ is possible to be bound by channel-coupling calculation. By contrast, the slope of the low-energy phase shifts of $\Lambda_c D^*$ is opposite to that of NJ/ψ channel, which means that the $\Lambda_c D^*$ is unbound even with channel coupling. All these results are also consistent with our previous bound-state calculation in Ref. [18].

TABLE IV: The mass and decay width (in MeV) of the $IJ^P = \frac{1}{2}\frac{3}{2}^-$ resonance states in the $N\Upsilon$ and $\Lambda_b B^*$ S -wave scattering process.

	two-channel coupling					
	$\Sigma_b B^*$		$\Sigma_b^* B$		$\Sigma_b^* B^*$	
	M	Γ	M	Γ	M	Γ
$N\Upsilon$	11126.3	1.7	11105.8	4.4	11155.7	3.8
$\Lambda_b B^*$	11125.5	0.9	11103.5	2.6	11152.0	2.7
	four-channel coupling					
	$\Sigma_b B^*$		$\Sigma_b^* B$		$\Sigma_b^* B^*$	
	M	Γ	M	Γ	M	Γ
$N\Upsilon$	11122.7	0.2	11103.6	0.8	nr	–
$\Lambda_b B^*$	11122.2	0.2	11102.4	0.3	11150.0	1.8

Because of the heavy flavor symmetry, we also extend the study to the hidden-bottom pentaquarks. The results are similar to the hidden-charm molecular pentaquarks. From Figs. 5 and 6, we can see that the $\Sigma_b B$, $\Sigma_b B^*$ and $\Sigma_b^* B^*$ states with $IJ^P = \frac{1}{2}\frac{1}{2}^-$ appear as resonance states in all scattering channels ($N\eta_b$, $N\Upsilon$, $\Lambda_b B$ and $\Lambda_b B^*$). The mass and decay width are illustrated in Table III. The resonance mass range of $\Sigma_b B$ state is 11077.2 ~ 11079.8 MeV and the decay width is about 1.6 MeV; $\Sigma_b B^*$ has the mass range of 11120.6 ~ 11125.8 MeV and the decay width of 3.0 MeV; and $\Sigma_b^* B^*$ has the mass range of 11141.5 ~ 11156.9 MeV and the decay width of 5.6 MeV. These results are qualitatively similar to the conclusion of Ref. [44], in which they predicted a few narrow N^* resonances with hidden beauty around 11 GeV in the coupled-channel unitary approach.

For the hidden-bottom pentaquarks with $IJ^P = \frac{1}{2}\frac{3}{2}^-$, both the states $\Sigma_b B^*$ and $\Sigma_b^* B$ appear as resonance states in the scattering phase shifts of $N\Upsilon$ and $\Lambda_b B^*$ channels. The $\Sigma_b^* B^*$ state appear as a resonance state only in the $\Lambda_b B^*$ scattering process. All the phase shifts are shown in Figs. 7 and 8. The mass and decay width are listed in Table IV, from which we can see that the $\Sigma_b B^*$ has the mass range of 11122.2 ~ 11122.7 MeV and the decay width of 0.4 MeV; and $\Sigma_b^* B$ has the mass range of 11102.4 ~ 11103.6 MeV and the decay width of 1.1 MeV. The resonance mass of $\Sigma_b^* B^*$ is 11150.0 MeV and the decay width is 1.8 MeV.

Similarly, the behaviour of the low-energy phase shifts of both $N\eta_b$ and $N\Upsilon$ also implies that $N\eta_b$ and $N\Upsilon$ with $IJ^P = \frac{1}{2}\frac{1}{2}^-$, as well as $N\Upsilon$ with $IJ^P = \frac{1}{2}\frac{3}{2}^-$ are all possible to be bound with channel-coupling.

IV. SUMMARY

In summary, we investigate the hidden-charm and hidden-bottom pentaquark resonances in the hadron-

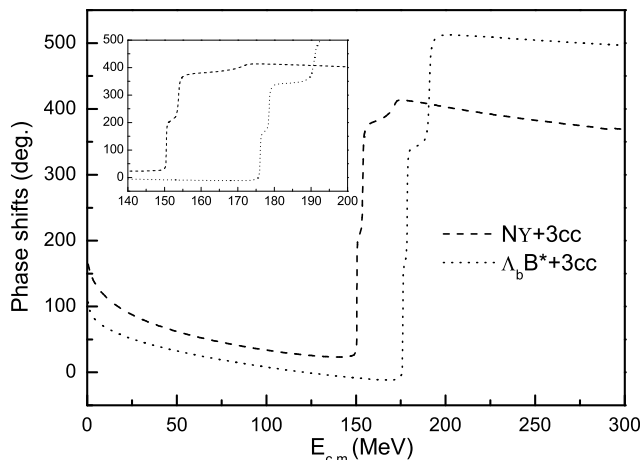


FIG. 8: The $N\Upsilon$ and $\Lambda_b B^*$ S -wave phase shifts with four-channel coupling for the $IJ^P = \frac{1}{2}\frac{3}{2}^-$ system.

hadron scattering process. For the hidden-charm sector, three resonance states with $IJ^P = \frac{1}{2}\frac{1}{2}^-$, as well as three resonance states with $IJ^P = \frac{1}{2}\frac{3}{2}^-$ are found to be dynamically generated from coupled scattering channels. Because of the hidden $c\bar{c}$ components involved in these states, the masses of these states are all above 4.2 GeV while their widths are only a few MeV. Extending to the hidden-bottom system, the results are similar. Both the resonance states with $IJ^P = \frac{1}{2}\frac{1}{2}^-$ and $IJ^P = \frac{1}{2}\frac{3}{2}^-$ are found from corresponding scattering process. The masses of these states are all above 11 GeV while their widths are only a few MeV. The nature of these states is sim-

ilar to the corresponding $N_{c\bar{c}}^*$ and $N_{b\bar{b}}^*$ states predicated in Ref. [4] and Ref. [44], which definitely cannot be accommodated by the conventional $3q$ quark models, and should form part of the heavy island for the quite stable N^* baryons.

Particularly, the behaviour of the low-energy phase shifts of the $N\eta_c$, NJ/ψ , $N\eta_b$ and $N\Upsilon$ indicates that the states $N\eta_c$, NJ/ψ , $N\eta_b$ and $N\Upsilon$ with $IJ^P = \frac{1}{2}\frac{1}{2}^-$, as well as NJ/ψ and $N\Upsilon$ with $IJ^P = \frac{1}{2}\frac{3}{2}^-$ are all possible to be bound by channel-coupling calculation.

All these heavy pentaquarks are worth searching in future experiments. Immediately after the LHCb, the Jefferson Lab proposed to look for the hidden-charm pentaquarks by using photo-production of J/ψ at threshold in Hall C [45]. Moreover, the pentaquarks with charm quarks can also be observed by the PANDA/FAIR [46]. For the pentaquarks with the hidden-bottom, we hope the proposed electron-ion collider (EIC) [47] and the Jefferson Lab [48] to discover these interesting super-heavy pentaquarks.

Acknowledgment

This work is supported partly by the National Science Foundation of China under Contract Nos. 11675080, 11775118 and 11535005, the Natural Science Foundation of the Jiangsu Higher Education Institutions of China (Grant No. 16KJB140006).

-
- [1] T. Nakano, *et al.* (LEPS Collaboration), *Phys. Rev. Lett.* **91**, 012002 (2003).
- [2] T. Nakano, *et al.* (LEPS Collaboration), *Phys. Rev. C* **79**, 025210 (2009).
- [3] Megumi Naruki for the J-PARC E19 Collaboration, Kyoto University, arXiv:1602.03951.
- [4] J. J. Wu, R. Molina, E. Oset, and B. S. Zou, *Phys. Rev. Lett.* **105**, 232001 (2010); *Phys. Rev. C* **84**, 015202 (2011).
- [5] Z. C. Yang, Z. F. Sun, J. He, X. Liu and S. L. Zhu, *Chin. Phys. C* **36**, 6 (2012).
- [6] C. W. Xiao, J. Nieves and E. Oset, *Phys. Rev. D* **88**, 056012 (2013).
- [7] T. Uchino, W. H. Liang and E. Oset, *Eur. Phys. J. A* **52**, 43 (2016).
- [8] M. Karliner and J. L. Rosner, *Phys. Rev. Lett.* **115**, 122001 (2015).
- [9] E. J. Garzon and J. J. Xie, *Phys. Rev. C* **92**, 035201 (2015).
- [10] W. L. Wang, F. Wang, Z. Y. Zhang and B. S. Zou, *Phys. Rev. C* **84**, 015203 (2011).
- [11] S. G. Yuan, K. W. We, J. He, H. S. Xu and B. S. Zou, *Eur. Phys. J. A* **48**, 61 (2012).
- [12] Y. Huang, J. He, H. F. Zhang and X. R. Chen, *J. Phys. G* **41**, 115004 (2014).
- [13] R. Aaij, *et al.* (LHCb Collaboration), *Phys. Rev. Lett.* **115**, 072001 (2015).
- [14] R. Chen, X. Liu, X. Q. Li and S. L. Zhu, *Phys. Rev. Lett.* **115**, 132002 (2015).
- [15] H. X. Chen, W. Chen, X. Liu, T. G. Steel and S. L. Zhu, *Phys. Rev. Lett.* **115**, 172001 (2015).
- [16] L. Roca, J. Nieves and E. Oset, *Phys. Rev. D* **92**, 094003 (2015).
- [17] J. He, *Phys. Lett. B* **753**, 547 (2016).
- [18] H. X. Huang, C. R. Deng, J. L. Ping and F. Wang, *Eur. Phys. J. C* **76**, 624 (2016).
- [19] G. Yang and J. L. Ping, *Phys. Rev. D* **95**, 014010 (2017).
- [20] U. G. Meissner and J. A. Oller, *Phys. Lett. B* **751**, 59 (2015).
- [21] C. W. Xiao and U. G. Meissner, *Phys. Rev. D* **92**, 114002 (2015).
- [22] R. Chen, X. Liu and S. L. Zhu, *Nucl. Phys. A* **954**, 406 (2016).
- [23] H. X. Chen, E. L. Cui, W. Chen, T. G. Steele, X. Liu and S. L. Zhu, *Eur. Phys. J. C* **76**, 572 (2016).
- [24] R. F. Lebed, *Phys. Lett. B* **749**, 454 (2015).
- [25] R. Zhu and C. F. Qiao, *Phys. Lett. B* **756**, 259 (2016).
- [26] L. Maiani, A. D. Polosa and V. Riquer, *Phys. Lett. B* **749**, 289 (2015).
- [27] V. V. Anisovich, M. A. Matveev, J. Nyiri, A. V. Sarant-

- sev and A. N. Semenova, arXiv:1507.07652.
- [28] R. Ghosh, A. Bhattacharya and B. Chakrabarti, arXiv:1508.00356.
- [29] Z. G. Wang, Eur. Phys. J. C **76**, 70 (2016).
- [30] A. Mironov and A. Morozov, JETP Lett. **102**, 271 (2015).
- [31] N. N. Scoccola, D. O. Riska and M. Rho, Phys. Rev. D **92**, 051501 (2015).
- [32] F. K. Guo, U. G. Meissner, W. Waang and Z. Yang, Phys. Rev. D **92**, 071502 (2015).
- [33] X. H. Liu, Q. Wang and Q. Zhao, Phys. Lett. B **757**, 231 (2016).
- [34] M. Mikhasenko, arXiv:1507.06552.
- [35] H. X. Chen, W. Chen, X. Liu and S. L. Zhu, Phys. Rep. **639**, 1-121 (2016).
- [36] J. L. Ping, H. X. Huang, H. R. Pang, F. Wang and C. W. Wong, Phys. Rev. C **79**, 024001 (2009).
- [37] H. Gao, H. Huang, T. Liu, J. Ping, F. Wang and Z. Zhao, Phys. Rev. C **95**, 055202 (2017).
- [38] F. Wang, G. H. Wu, L. J. Teng and T. Goldman, Phys. Rev. Lett. **69**, 2901 (1992); G. H. Wu, L. J. Teng, J. L. Ping, F. Wang and T. Goldman, Phys. Rev. C **53**, 1161 (1996).
- [39] H. X. Huang, P. Xu, J. L. Ping and F. Wang, Phys. Rev. C **84**, 064001 (2011).
- [40] M. Kamimura, Supp. Prog. Theo. Phys. **62**, 236 (1977).
- [41] J. L. Ping, F. Wang and T. Goldman, Nucl. Phys. A **657**, 95 (1999); G. H. Wu, J. L. Ping, L. J. Teng *et al.*, Nucl. Phys. A **673**, 279 (2000); H. R. Pang, J. L. Ping, F. Wang and T. Goldman, Phys. Rev. C **65**, 014003 (2001); J. L. Ping, F. Wang and T. Goldman, Nucl. Phys. A **688**, 871 (2001); J. L. Ping, H. R. Pang, F. Wang and T. Goldman, Phys. Rev. C **65**, 044003 (2002).
- [42] A. Valcarce, H. Garcilazo, F. Fernandez and P. Gonzalez, Rep. prog. Phys. **68**, 965 (2005) and reference there in.
- [43] J. Vijande, F. Fernandez and A. Valcarce, J. Phys. G **31**, 481 (2005).
- [44] J. J. Wu, L. Zhao, and B. S. Zou, Phys. Lett. B **709**, 70 (2012).
- [45] Z.-E. Meziani, *et al.* (JLab Collaboration), arXiv:1609.00676v2.
- [46] M. F. M. Lutz *et al* (PANDA Collaboration), arXiv:0903.3905.
- [47] V. Ptitsyn, AIP Conf. Proc. **735**, 1149 (2009).
- [48] S. Joosten and Z.-E. Meziani, arXiv:1802.02616v2.